Modeling and static optimization of a variable speed pumped storage power plant

authored by **J. Schmidt, W. Kemmetmüller, and A. Kugi**

and published in *Renewable Energy*.

Cite this article as:

J. Schmidt, W. Kemmetmüller, and A. Kugi, "Modeling and static optimization of a variable speed pumped storage power plant", *Renewable Energy*, vol. 111, pp. 38–51, 2017. DOI: https://dx.doi.org/10.1016/j.renene.2017.03.055

BibTex entry:

```
% Encoding: windows-1252

@Article{Schmidt_2017_Renewable_Energy,
  author = {Schmidt, J. and Kemmetm\"uller, W. and Kugi, A.},
  title = {{M}odeling and static optimization of a variable speed pumped storage power plant},
  journal = {Renewable Energy},
  year = {2017},
  volume = {111},
  pages = {38-51},
  doi = {https://dx.doi.org/10.1016/j.renene.2017.03.055},
}

@Comment{jabref-meta: databaseType:bibtex;}
```

Link to original paper:

http://dx.doi.org/https://dx.doi.org/10.1016/j.renene.2017.03.055

Contact:

Automation and Control Institute (ACIN)
Vienna University of Technology
Gusshausstrasse 27-29/E376
1040 Vienna, Austria

Internet: www.acin.tuwien.ac.at
E-mail: office@acin.tuwien.ac.at
Phone: +43 1 58801 37601
Fax: +43 1 58801 37699

Modeling and Static Optimization of a Variable Speed Pumped Storage Power Plant

J. Schmidt*, W. Kemmetmüller*, A. Kugi*

Automation and Control Institute, Vienna University of Technology, Gußhausstraße 27–29, 1040 Vienna, Austria

Abstract

Pumped storage power plants are key components to stabilize electric distribution networks with high amount of intermittent power sources as, e.g., solar and wind power plants. Tailored mathematical models are important for the transient and the stationary analysis of such plants. A comprehensive mathematical model of a variable speed operated pumped storage power plant, which incorporates reversible pump turbines in combination with doubly fed induction machines, is developed in this paper. Special emphasis is laid on an accurate description of important dynamic effects (e.g., water hammer) and of the energy losses of the system. Based on this model, optimal stationary operating points are determined, which minimize the overall system losses and systematically take into account the operating constraints.

Keywords: variable speed pumped storage power plant, doubly fed induction machine, mathematical modeling, optimal stationary operation

1. Introduction

Electric power industry is currently faced with environmental issues, increasing energy consumption and limited resources of fossil fuels. These challenges are, amongst others, tackled by an intensified usage of renewable energy sources, in particular wind and sun. The intermittent nature of these energy sources calls for a sufficient amount of large scale energy storage capabilities in order to ensure a generation-load balance and thus grid stability. The well-established pumped storage power plants (PSPPs) still represent the most attractive way of large scale energy storage, having a worldwide installed capacity of approximately 130 GW [1]. In particular variable speed operated PSPPs with reversible pump turbines offer distinct advantages in comparison to conventional fixed-speed PSPPs, including: (i) increased efficiency (especially during part-load operation) and an enhanced operating range in turbine mode, (ii) improved network frequency regulation capabilities due to rapid injection of active power (flywheel effect) as well as (iii) improved active power regulation capability during pump operation, see, e.g., [2, 3, 4, 5].

Together with the ability of reactive power control, these features make variable speed PSPPs an excellent aid for improving grid stability, e.g., by primary frequency control. Two types of variable speed PSPPs are typically considered in literature: the doubly fed induction machine (DFIM) with a part-load converter at the rotor terminals and the synchronous machine with a full-load converter at the stator terminals [5, 6, 7]. The converter fed synchronous machine inherently offers some advantages over the DFIM, including a much larger possible speed range [7]. While power electronics components typically limit the power range of a full-load converter, the recent advances in power electronics technology allow to build such PSPPs with ever increasing power, see, e.g., [8] where a commissioned PSPP applying a 100 MW full-load converter is described.

Nevertheless, the usual restriction of the speed range to approximately $\pm 10\,\%$ around the synchronous speed allows to size the part-load converter of the DFIM topology to only a small portion of the rated machine power. This constitutes a decisive economic advantage of the DFIM topology, currently making it the predominant technology for high power ($\gtrsim 100\,$MW) applications, with several examples of commissioned power plants, see, e.g., [9, 10, 11]. Hence it is a variable speed PSPP employing the DFIM topology that is considered in the present contribution.

Mathematical models of the PSPP are required for the dynamic simulation, the controller design and the optimization of the operation of PSPPs. Thus, one goal of this contribution is the derivation of a comprehensive mathematical model of a variable speed PSPP. In particular, special focus is laid on the accurate description of the dynamic behavior as well as of the losses of the overall plant, incorporating both the mechanic as well as the electric key components. In literature, see, e.g., [10, 12, 13], simplified pump turbine models are often used, which are not suitable to properly reflect pump turbine losses in a larger operating range. A more sophisticated PSPP model intended for power system simulations is presented in [14].

*Corresponding author. *Tel.:* +43 1 58801 376296, *Fax:* +43 1 58801 9376296.

Email addresses: schmidt@acin.tuwien.ac.at (J. Schmidt), kemmetmueller@acin.tuwien.ac.at (W. Kemmetmüller), kugi@acin.tuwien.ac.at (A. Kugi)

Preprint submitted to Renewable Energy *April 12, 2017*

Post-print version of the article: J. Schmidt, W. Kemmetmüller, and A. Kugi, "Modeling and static optimization of a variable speed pumped storage power plant", *Renewable Energy*, vol. 111, pp. 38–51, 2017. DOI: https://dx.doi.org/10.1016/j.renene.2017.03.055
The content of this post-print version is identical to the published paper but without the publisher's final layout or copy editing.

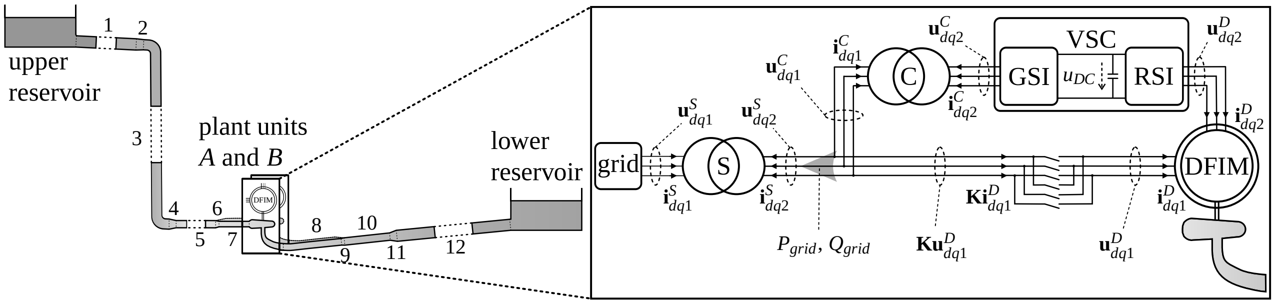

Figure 1: Setup of the considered variable speed pumped storage power plant (PSPP). The pipe segment numbering corresponds to Table 3. The electric system of each plant consists of a DFIM, a step-up transformer (S), a converter transformer (C) and a voltage-source converter (VSC), comprising a grid side inverter (GSI) and a rotor side inverter (RSI). Vector notation is applied for the respective dq-quantities, e.g., $\mathbf{u}^D_{dq1} = \begin{bmatrix} u^D_{d1} & u^D_{q1} \end{bmatrix}^{\mathrm{T}}$.

Here, the hydraulic system is modeled in a similar way as in this paper, i.e. modeling the pump turbine in a quasi-stationary manner by its characteristics and numerically solving the pipe model's partial differential equations (PDEs) by the Method of Characteristics (MOC). The mathematical model of the electric system, however, is not described in detail. This might be reasonable for power system simulations, but is not appropriate for controller design and optimization. In [4] a variable speed PSPP is modeled based on the hydraulic modeling approach of [15, 16], which applies a finite difference scheme for the numerical solution of the pipe PDEs. The simulation builds upon an existing software tool, which was originally developed for the simulation of electric systems [16]. Thus, also the hydraulic components are described by equivalent electric models. As the pump turbine characteristics are interpolated with continuity of order 0, it is, however, difficult to directly use this model for optimization purposes. In [17] a simulation model based on the MOC and a continuously differentiable surface interpolation of the pump turbine characteristics [18] is applied for water hammer studies. This modeling approach is also described in [19]. A continuously differentiable interpolation of the pump turbine characteristics allows for the application of numerically efficient gradient based optimization methods. Therefore, a similar interpolation scheme is also provided in the present work, combining a state-of-the-art modeling approach of the hydraulic system with a detailed model of the electric system, particularly modeling the energy losses of the electric subsystem in more detail compared to above mentioned works.

Since PSPPs involve remarkable investments, suitable building sites are limited and due to liberalized energy markets, efficient operation is becoming increasingly important. In particular, the additional degree of freedom gained from variable speed operation is utilized to increase the efficiency of hydraulic machines. Reference [20] briefly describes the determination of optimal stationary operating points of a hydro power plant, where the hydraulic components and the generators are taken into account in a special software tool. Stationary operating points of maximum efficiency are determined by an iterative process. Since the generators are modeled as active power-depending efficiencies, their operating constraints are not systematically considered in the optimization process. In [4] control strategies for the optimized stationary operation of variable speed pump turbines are suggested. In turbine mode, the optimal set point of the turbine speed is determined for a given net head and a desired output power from a lookup table. Similarly, in pumping mode an optimal guide vane opening is calculated for a given rotational velocity and a given net head by a stationary law. In these cases, operating constraints are not explicitly taken into account and in [4] optimality is solely based on the pump turbine characteristics.

The mathematical model proposed in this paper is intended to serve as a basis for the analysis of the static and dynamic system behavior (e.g., water hammer studies), the design and test of control strategies and the determination of optimal system operation. In this paper, the model is used to calculate optimal stationary operating points of the PSPP for different modes of operation, which yield minimal energy losses of the overall system while adhering to operating constraints.

The paper is organized as follows: Section 2 introduces the considered variable speed PSPP and summarizes the mathematical models of its components. In Section 3, the dynamic behavior of the PSPP is analyzed by simulation studies. Section 4 describes the optimization problem for optimal stationary operating points and presents its numerical results. Finally, Section 5 gives some conclusions.

2. Mathematical Model

The overall system, depicted in Fig. 1, consists of two plant units A and B, which are coupled by a common pipe system. Assuming constant grid voltage amplitude and frequency, the coupling over the common electric grid segment can be neglected. Further, it is assumed that both plant units have an identical configuration, which allows to apply the same mathematical model to both plant units. If necessary, the superscripts A and B are utilized to distinguish the different plant units. Subsequently, quantities in per unit representation are often used, which will be marked by $\tilde{(\cdot)}$.

2.1. Electric Subsystem

The equations of the electric system are given in a per unit dq-representation, normalized with respect to the stator of the DFIM. The reference frame is synchronously rotating with the constant grid frequency $\omega_{grid} = 2\,\pi 50\,\mathrm{rad/s}$, which is also used as the base frequency ω_b in the per unit representation, i.e. $\omega_b = \omega_{grid}$, see Table 1. The respective 0-components are not taken into consideration, since they do not influence the dynamic behavior of the system. The base values of power S_b and voltage u_b for the per unit representation of the electric subsystem are derived from the rated stator values of the DFIM, see Table 1. The other base quantities are selected in accordance to [21], e.g., the base current and the base torque read as

$$i_b = \frac{2}{3}\frac{S_b}{u_b} \quad \text{and} \quad T_b = \frac{n_{pp} S_b}{\omega_b}, \tag{1}$$

see Table 1, with the number of pole pairs $n_{pp} = 7$.

Table 1: Base quantities.

Description	Parameter	Value	Unit
apparent power	S_b	182.50	MVA
peak value of phase voltage	u_b	$15\sqrt{\frac{2}{3}}$	kV
phase current	i_b	9.93	kA
grid frequency	ω_b	$2\pi 50$	rad/s
torque	T_b	4.07	MNm

The electric grid is modeled as a balanced three-phase voltage source of constant amplitude $\tilde{u}_{grid} = 1$ and, as already mentioned before, a constant angular frequency $\omega_{grid} = 2\,\pi 50\,\mathrm{rad/s}$. The corresponding dq-components of the grid voltage are constant and coincide with the dq-components $\tilde{u}^S_{d1}$, $\tilde{u}^S_{q1}$ of the step-up transformer, see Fig. 1. Using proper alignment between grid voltage and the reference frame, these voltages can be written as

$$\tilde{u}^S_{d1} = \tilde{u}_{grid} = 1, \quad \tilde{u}^S_{q1} = 0. \tag{2}$$

The electric system of each plant incorporates a DFIM (D), a step-up transformer (S), a converter transformer (C) and a voltage source converter (VSC), see Fig. 1. The transformers are necessary to adjust the corresponding voltage levels. As discussed before, the DFIM can operate both in generator mode (turbine mode) and motor mode (pumping mode). To allow for operation in both directions of rotation, switching facilities are incorporated to reverse the phase order at the stator terminals, see, e.g., [22]. The start-up of the DFIM and the transition between pumping and turbine mode require additional measures, both in the electric and the hydraulic system, see, e.g., [23, 24]. These operations are, however, not considered in this contribution and thus not further discussed.

A magnetically linear model, which includes the influence of iron losses, is used to describe the dynamic behavior of the DFIM, see, e.g., [25, 26]. The differential equations for the stator flux components $\tilde{\psi}^D_{d1}$ and $\tilde{\psi}^D_{q1}$ read as

$$\frac{1}{\omega_b}\frac{\mathrm{d}\tilde{\psi}^D_{d1}}{\mathrm{d}t} = -\tilde{R}^D_1 \tilde{i}^D_{d1} + \tilde{\omega}^D_{syn}\tilde{\psi}^D_{q1} + \tilde{u}^D_{d1} \tag{3a}$$

$$\frac{1}{\omega_b}\frac{\mathrm{d}\tilde{\psi}^D_{q1}}{\mathrm{d}t} = -\tilde{R}^D_1 \tilde{i}^D_{q1} - \tilde{\omega}^D_{syn}\tilde{\psi}^D_{d1} + \tilde{u}^D_{q1}, \tag{3b}$$

with the stator resistance $\tilde{R}^D_1$, the components $\tilde{i}^D_{d1}$ and $\tilde{i}^D_{q1}$ of the stator currents, and the components $\tilde{u}^D_{d1}$ and $\tilde{u}^D_{q1}$ of the stator voltages. Moreover, $\tilde{\omega}^D_{syn}$ is equal to the sign of the rotation frequency $\tilde{\omega}$ of the rotor, i.e. $\tilde{\omega}^D_{syn} = \mathrm{sign}(\tilde{\omega})$. The rotor fluxes $\tilde{\psi}^D_{d2}$ and $\tilde{\psi}^D_{q2}$ are given in an equivalent form

$$\frac{1}{\omega_b}\frac{\mathrm{d}\tilde{\psi}^D_{d2}}{\mathrm{d}t} = -\tilde{R}^D_2 \tilde{i}^D_{d2} + \left(\tilde{\omega}^D_{syn} - \tilde{\omega}\right)\tilde{\psi}^D_{q2} + \tilde{u}^D_{d2} \tag{4a}$$

$$\frac{1}{\omega_b}\frac{\mathrm{d}\tilde{\psi}^D_{q2}}{\mathrm{d}t} = -\tilde{R}^D_2 \tilde{i}^D_{q2} - \left(\tilde{\omega}^D_{syn} - \tilde{\omega}\right)\tilde{\psi}^D_{d2} + \tilde{u}^D_{q2}. \tag{4b}$$

Here, $\tilde{R}^D_2$ is the rotor resistance, $\tilde{i}^D_{d2}$ and $\tilde{i}^D_{q2}$ denote the rotor current components, and $\tilde{u}^D_{d2}$ and $\tilde{u}^D_{q2}$ are the corresponding rotor voltage components. The dynamic model of the DFIM is completed by the differential equations, see, e.g., [25, 26]

$$\frac{1}{\omega_b}\frac{\mathrm{d}\tilde{\psi}^D_{dm}}{\mathrm{d}t} = -\tilde{R}^D_i\left(\tilde{i}^D_{dm} - \tilde{i}^D_{d1} - \tilde{i}^D_{d2}\right) + \tilde{\omega}^D_{syn}\tilde{\psi}^D_{qm} \tag{5a}$$

$$\frac{1}{\omega_b}\frac{\mathrm{d}\tilde{\psi}^D_{qm}}{\mathrm{d}t} = -\tilde{R}^D_i\left(\tilde{i}^D_{qm} - \tilde{i}^D_{q1} - \tilde{i}^D_{q2}\right) - \tilde{\omega}^D_{syn}\tilde{\psi}^D_{dm}, \tag{5b}$$

describing the magnetization flux components $\tilde{\psi}^D_{dm}$ and $\tilde{\psi}^D_{qm}$ as functions of the magnetization current components $\tilde{i}^D_{dm}$ and $\tilde{i}^D_{qm}$ and the stator and rotor current components. Therein, the resistance $\tilde{R}^D_i$ is used to represent the iron losses of the DFIM. The fluxes of the DFIM are connected with the currents in the form

$$\begin{aligned}
\tilde{\psi}^D_{d1} &= \tilde{\psi}^D_{dm} + \tilde{L}^D_1\tilde{i}^D_{d1} & \tilde{\psi}^D_{q1} &= \tilde{\psi}^D_{qm} + \tilde{L}^D_1\tilde{i}^D_{q1} \\
\tilde{\psi}^D_{d2} &= \tilde{\psi}^D_{dm} + \tilde{L}^D_2\tilde{i}^D_{d2} & \tilde{\psi}^D_{q2} &= \tilde{\psi}^D_{qm} + \tilde{L}^D_2\tilde{i}^D_{q2} \\
\tilde{\psi}^D_{dm} &= \tilde{L}^D_m\tilde{i}^D_{dm} & \tilde{\psi}^D_{qm} &= \tilde{L}^D_m\tilde{i}^D_{qm},
\end{aligned} \tag{6}$$

with the leakage inductances $\tilde{L}^D_1$ and $\tilde{L}^D_2$ of the stator and rotor, respectively, and the magnetization inductance $\tilde{L}^D_m$. Finally, the torque $\tilde{T}$ of the DFIM reads as

$$\tilde{T} = \tilde{L}^D_m(\tilde{i}^D_{d2}\tilde{i}^D_{qm} - \tilde{i}^D_{q2}\tilde{i}^D_{dm}). \tag{7}$$

The mathematical models of the converter transformer (superscript C) and the step-up transformer (superscript

Post-print version of the article: J. Schmidt, W. Kemmetmüller, and A. Kugi, "Modeling and static optimization of a variable speed pumped storage power plant", *Renewable Energy*, vol. 111, pp. 38–51, 2017. DOI: https://dx.doi.org/10.1016/j.renene.2017.03.055
The content of this post-print version is identical to the published paper but without the publisher's final layout or copy editing.

S) are directly obtained from the model of the DFIM (3)-(6) by setting $\tilde{\omega} = 0$, $\tilde{\omega}^S_{syn} = \tilde{\omega}^C_{syn} = 1$ and exchanging superscripts. Different to the stator and rotor windings of the machine, the transformer windings are connected in the vector group Yd5. This is incorporated into the model by multiplying the voltages and currents of the secondary side by appropriate constant rotation matrices, see, e.g., [27].

The frequency converter is the essential component to allow for a variable speed operation of the pumped storage plant. There are a number of possible converter topologies available in the medium voltage range and for the required power ratings of approx. 20 MVA [28]. These converter topologies certainly have large differences in their setup and the control strategies used to operate them. However, the objective of the mathematical model derived in this paper is to describe the essential dynamic behavior of the overall pumped storage plant. Thus, a rather generic approach, which is capable of describing the average behavior of many converter topologies, is used. It is an extension of the so-called fundamental frequency or pseudo continuous converter model, see, e.g., [4, 29] and based on the following assumptions:

- a back-to-back voltage source converter topology is used and
- the switching rate of the VSC is much faster than the remaining dynamics of the electric system.

The converter allows to directly assign the average voltage components $\tilde{u}^C_{d2}$, $\tilde{u}^C_{q2}$ at the secondary side of the converter transformer and $\tilde{u}^D_{d2}$, $\tilde{u}^D_{q2}$ at the rotor of the machine within certain limits.

Simplifying the results in [30], the losses of the grid side inverter (GSI) and the rotor side inverter (RSI) are approximated by

$$\tilde{P}_{GSI} = \tilde{k}_{GSI,0} + \tilde{k}_{GSI,1}\tilde{i}^C_2 + \tilde{k}_{GSI,2}\left(\tilde{i}^C_2\right)^2 \tag{8a}$$
$$\tilde{P}_{RSI} = \tilde{k}_{RSI,0} + \tilde{k}_{RSI,1}\tilde{i}^D_2 + \tilde{k}_{RSI,2}\left(\tilde{i}^D_2\right)^2 \tag{8b}$$

with the current magnitudes

$$\tilde{i}^C_2 = \sqrt{\left(\tilde{i}^C_{d2}\right)^2 + \left(\tilde{i}^C_{q2}\right)^2} \text{ and } \tilde{i}^D_2 = \sqrt{\left(\tilde{i}^D_{d2}\right)^2 + \left(\tilde{i}^D_{q2}\right)^2}, \tag{9}$$

and estimated parameters $\tilde{k}_{GSI,j}$, $\tilde{k}_{RSI,j}$, $j = 0, 1, 2$. The power $\tilde{P}^C_2$ and $\tilde{P}^D_2$ transferred by the converter to the transformer and the DFIM, respectively, read as

$$\tilde{P}^C_2 = \tilde{u}^C_{d2}\tilde{i}^C_{d2} + \tilde{u}^C_{q2}\tilde{i}^C_{q2} \text{ and } \tilde{P}^D_2 = \tilde{u}^D_{d2}\tilde{i}^D_{d2} + \tilde{u}^D_{q2}\tilde{i}^D_{q2}. \tag{10}$$

Using the balance of energy, the dynamics of the DC-link voltage $\tilde{u}_{DC}$ can be written in the form

$$\frac{1}{\omega_b}\frac{\mathrm{d}\tilde{u}^2_{DC}}{\mathrm{d}t} = -\frac{3}{\tilde{C}_{DC}}\left(\tilde{P}^C_2 + \tilde{P}_{GSI} + \tilde{P}^D_2 + \tilde{P}_{RSI}\right), \tag{11}$$

with the effective DC-link capacitance $\tilde{C}_{DC}$.

The mathematical model of the electric system is completed by the electric interconnection of the transformators and the DFIM in form of the following constraints, see Fig. 1:

1. The voltages at the common node are equal, i.e., in terms of phase voltages of the three-phase system,
$$\begin{bmatrix}\tilde{u}^S_{a2}\\ \tilde{u}^S_{b2}\\ \tilde{u}^S_{c2}\end{bmatrix} = \begin{bmatrix}\tilde{u}^D_{a1}\\ \tilde{u}^D_{b1}\\ \tilde{u}^D_{c1}\end{bmatrix} \quad \text{or} \quad \begin{bmatrix}\tilde{u}^S_{a2}\\ \tilde{u}^S_{b2}\\ \tilde{u}^S_{c2}\end{bmatrix} = \begin{bmatrix}\tilde{u}^D_{a1}\\ \tilde{u}^D_{c1}\\ \tilde{u}^D_{b1}\end{bmatrix} \tag{12}$$
holds, depending on the switching state at the stator terminals of the DFIM. Neglecting the 0-components, this reads as
$$\begin{bmatrix}\tilde{u}^S_{d2}\\ \tilde{u}^S_{q2}\end{bmatrix} = \begin{bmatrix}\tilde{u}^C_{d1}\\ \tilde{u}^C_{q1}\end{bmatrix} = \mathbf{K}\begin{bmatrix}\tilde{u}^D_{d1}\\ \tilde{u}^D_{q1}\end{bmatrix} \tag{13}$$
in dq-representation, with $\mathbf{K} = \mathrm{diag}[1, \mathrm{sign}(\tilde{\omega})]$.
2. The sum of the currents at the common node is zero
$$\begin{bmatrix}\tilde{i}^S_{d2}\\ \tilde{i}^S_{q2}\end{bmatrix} + \begin{bmatrix}\tilde{i}^C_{d1}\\ \tilde{i}^C_{q1}\end{bmatrix} + \mathbf{K}\begin{bmatrix}\tilde{i}^D_{d1}\\ \tilde{i}^D_{q1}\end{bmatrix} = \begin{bmatrix}0\\ 0\end{bmatrix}, \tag{14}$$
which implies that only four of the six currents are independent. In the following, $\tilde{i}^S_{d2}$ and $\tilde{i}^S_{q2}$ are chosen as the dependent currents.

The resulting mathematical model of the interconnected electric components can be represented in the form

$$\frac{1}{\omega_b}\frac{\mathrm{d}\mathbf{x}_e}{\mathrm{d}t} = \mathbf{g}_e\left(\mathbf{x}_e, \tilde{\omega}, \mathbf{u}_e, \mathbf{u}_{grid}\right) \tag{15}$$

with

$$\mathbf{x}^{\mathrm{T}}_e = [\tilde{i}^S_{d1}, \tilde{i}^S_{q1}, \tilde{i}^S_{dm}, \tilde{i}^S_{qm}, \tilde{i}^C_{d1}, \tilde{i}^C_{q1}, \tilde{i}^C_{d2}, \tilde{i}^C_{q2}, \tilde{i}^C_{dm}, \tilde{i}^C_{qm}, \tilde{i}^D_{d1}, \tilde{i}^D_{q1}, \tilde{i}^D_{d2}, \tilde{i}^D_{q2}, \tilde{i}^D_{dm}, \tilde{i}^D_{qm}, \tilde{u}_{DC}], \tag{16a}$$
$$\mathbf{u}^{\mathrm{T}}_e = [\tilde{u}^C_{d2}, \tilde{u}^C_{q2}, \tilde{u}^D_{d2}, \tilde{u}^D_{q2}]. \tag{16b}$$

The corresponding active and reactive power output of the pumped storage plant to the grid $\tilde{P}_{grid}$, $\tilde{Q}_{grid}$ are defined at the secondary side of the step-up transformer by[1]

$$\tilde{P}_{grid} = -\tilde{u}^D_{d1}\tilde{i}^D_{d1} - \tilde{u}^D_{q1}\tilde{i}^D_{q1} - \tilde{u}^C_{d1}\tilde{i}^C_{d1} - \tilde{u}^C_{q1}\tilde{i}^C_{q1} \tag{17a}$$
$$\tilde{Q}_{grid} = \left(\tilde{u}^D_{d1}\tilde{i}^D_{q1} - \tilde{u}^D_{q1}\tilde{i}^D_{d1}\right)\mathrm{sign}(\tilde{\omega}) + \tilde{u}^C_{d1}\tilde{i}^C_{q1} - \tilde{u}^C_{q1}\tilde{i}^C_{d1}. \tag{17b}$$

2.2. Hydraulic Subsystem

The hydraulic system of the pumped storage power plant consists of two reservoirs which are connected to two Francis turbines via a hydraulic pipe system, see Fig. 1. The hydraulic system is responsible for a major part of the

[1] In these equations, the voltages are functions of the system state $\mathbf{x}_e$, i.e. $\tilde{u}^D_{d1} = \tilde{u}^D_{d1}(\mathbf{x}_e)$, $\tilde{u}^D_{q1} = \tilde{u}^D_{q1}(\mathbf{x}_e)$, $\tilde{u}^C_{d1} = \tilde{u}^C_{d1}(\mathbf{x}_e)$ and $\tilde{u}^C_{q1} = \tilde{u}^C_{q1}(\mathbf{x}_e)$.

Post-print version of the article: J. Schmidt, W. Kemmetmüller, and A. Kugi, "Modeling and static optimization of a variable speed pumped storage power plant", *Renewable Energy*, vol. 111, pp. 38–51, 2017. DOI: https://dx.doi.org/10.1016/j.renene.2017.03.055
The content of this post-print version is identical to the published paper but without the publisher's final layout or copy editing.

dynamics and losses of the system. Thus, special emphasis is laid on an accurate modeling of the hydraulic components.

The central hydraulic component is the Francis turbine, which operates both in pumping and turbine mode. Since the transients of the pressures and volume flows inside the turbine are considerably faster than the dynamics of the remaining hydraulic system, it is possible to describe its behavior by a quasi-stationary characteristics, see, e.g., [16, 31, 32]. It is common practice in literature to represent the turbine characteristics by using the specific speed N_{11}, the specific volume flow q_{11} and the specific torque T_{11}, which are related to the physical quantities in the form

$$N_{11} = \frac{ND_r}{\sqrt{H_n}}, \quad q_{11} = \frac{q_{PT}}{D_r^2\sqrt{H_n}}, \quad T_{11} = \frac{T_{PT}}{D_r^3 H_n}, \tag{18}$$

see, e.g., [4, 33]. Here, N is the rotational speed, q_{PT} is the volume flow, T_{PT} describes the torque and D_r is the reference diameter of the turbine. Further, the net head H_n (also called dynamic head) is defined as

$$H_n = \frac{p_{US} - p_{DS}}{\rho g} + \Delta z + \frac{v_{US}^2 - v_{DS}^2}{2g}, \tag{19}$$

with the fluid mass density ρ, the gravitational acceleration $g = 9.81\,\mathrm{m}^2/\mathrm{s}$, the upstream pressure p_{US}, the downstream pressure p_{DS}, the corresponding fluid velocities v_{US} and v_{DS} as well as the height difference $\Delta z = z_{US} - z_{DS}$ between the inlet and the outlet of the turbine, see, e.g., [31]. Fig. 2 shows the measured characteristic maps of the Francis turbine as a function of the guide vane opening χ. Here, the quantities are normalized to the operating point of best turbine efficiency, which is characterized by χ_r, $N_{11,r}$, $q_{11,r}$, $T_{11,r}$.

The S-shape characteristics in the transition from turbine mode ($N_{11}, q_{11}, T_{11} > 0$) to the inverse pumping mode ($N_{11} > 0$, $q_{11}, T_{11} < 0$) is problematic for the interpolation of the data points in a simulation model due to ambiguous operating points for the same values of χ and N_{11}. To circumvent this problem, the polar coordinates r and θ are introduced in the form

$$r^2 = \left(\frac{N_{11}}{N_{11,r}}\right)^2 + \left(\frac{q_{11}}{q_{11,r}}\right)^2 = \frac{H_{n,r}}{H_n} f(N, q_{PT}), \tag{20a}$$

$$\theta = \arctan\left(\frac{\frac{q_{11}}{q_{11,r}}}{\frac{N_{11}}{N_{11,r}}}\right) = \arctan\left(\frac{\frac{q_{PT}}{q_{PT,r}}}{\frac{N}{N_r}}\right), \tag{20b}$$

see, e.g., [16]. Here, the abbreviation $f(N, q_{PT})$ reads as

$$f(N, q_{PT}) = \left(\frac{N}{N_r}\right)^2 + \left(\frac{q_{PT}}{q_{PT,r}}\right)^2, \tag{21}$$

and the reference values $q_{PT,r}$, $H_{n,r}$, $T_{PT,r}$ can be calculated from the best efficiency point by (18) for a given value of $N = N_r$. In this work, N_r is chosen[2] as the synchronous rotational speed of the DFIM, see Table 2 for a definition

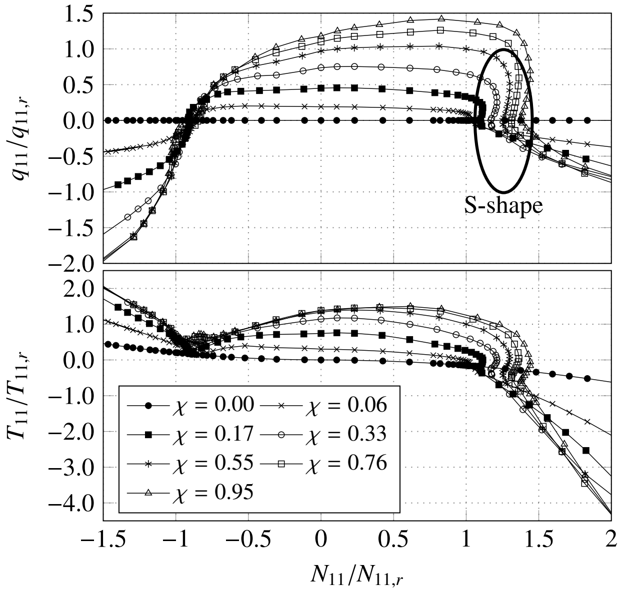

Figure 2: Normalized characteristic maps of the Francis turbine, parametrized by the guide vane opening χ.

Table 2: Pump turbine parameters.

Parameter	**Value**	**Unit**
$N_{11,r}$	81.37	rpm
$q_{11,r}$	0.20	m^3/s
$T_{11,r}$	211.05	N m
χ_r	0.55	
N_r	428.57	rpm
$H_{n,r}$	355.53	m
$q_{PT,r}$	47.59	m^3/s
$T_{PT,r}$	3.44	MNm
D_r	3.58	m
Δz	11.50	m

of the pump turbine parameters. Using these new coordinates allows to calculate the transformed charactistic maps in the form

$$W_H = \frac{1}{r^2} = \frac{\frac{H_n}{H_{n,r}}}{f(N, q_{PT})} \tag{22a}$$

$$W_B = W_H \frac{T_{11}}{T_{11,r}} = \frac{\frac{T_{PT}}{T_{PT,r}}}{f(N, q_{PT})}, \tag{22b}$$

see, e.g., [16, 31], which are shown in Fig. 3. While this transformation eliminates the problem with ambiguous operating points, it is no longer possible to represent the case of a fully closed guide vane $\chi = 0$ by the transformed

[2] Instead of choosing N_r, it would also be possible to choose $H_{n,r}$, e.g., as the nominal value of the net head.

Post-print version of the article: J. Schmidt, W. Kemmetmüller, and A. Kugi, “Modeling and static optimization of a variable speed pumped storage power plant”, *Renewable Energy*, vol. 111, pp. 38–51, 2017. DOI: https://dx.doi.org/10.1016/j.renene.2017.03.055
The content of this post-print version is identical to the published paper but without the publisher’s final layout or copy editing.

characteristic maps. This case is, however, only of minor practical interest and thus not considered in this paper. As already discussed before, an at least continuously differentiable approximation of the characteristic maps is required for the simulation model and for the usage in gradient based optimization strategies. In this work, cubic B-Spline surface interpolation based on surface skinning [34] was applied. The resulting interpolated characteristic maps are given together with the measured data points in Fig. 3.

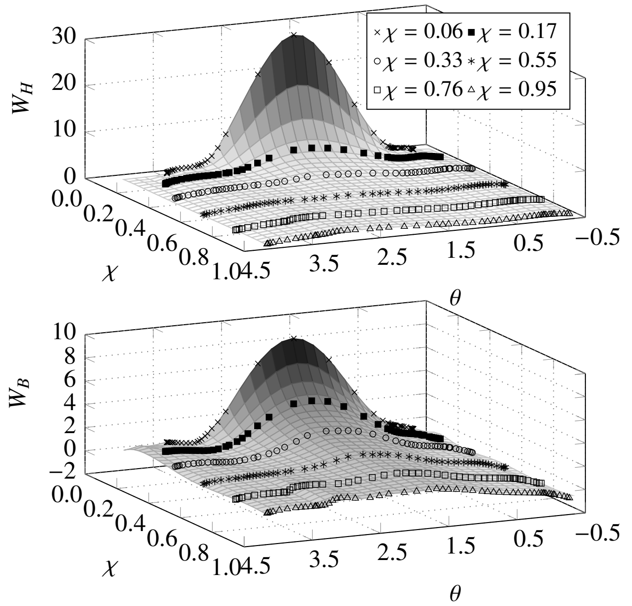

Figure 3: Transformed pump turbine data points from Fig. 2 and interpolated characteristic maps $W_H(\chi, \theta)$ and $W_B(\chi, \theta)$.

Using (22), the net head H_n and the pump turbine torque T_{PT}

$$H_n(\chi, N, q_{PT}) = H_{n,r} W_H(\chi, \theta(N, q_{PT})) f(N, q_{PT}), \tag{23a}$$

$$T_{PT}(\chi, N, q_{PT}) = T_{PT,r} W_B(\chi, \theta(N, q_{PT})) f(N, q_{PT}) \tag{23b}$$

are defined for given volume flow q_{PT}, rotary speed N and guide vane position χ of the pump turbine.

Note that in [18] the specific quantities N_{11}, q_{11} and T_{11} are interpolated on B-Spline surfaces, which allows to represent fully closed guide vanes. In some circumstances, however, it might be considered a drawback, that instead of θ a more general parametrization variable has to be applied, which doesn't have an immediate relationship to any physical variable of the system.

The pump turbines of the power plant are connected to the upper and lower reservoir by an arrangement of pipe segments, cf. Fig. 1. Assuming a one-dimensional axial flow, a single pipe segment is modeled by the PDEs for the pressure p and the fluid velocity $v = \frac{q}{A}$ in the form, see, e.g., [31, 35, 36, 37]

$$\frac{1}{\rho a^2}\left(\frac{\partial p}{\partial t} + v\frac{\partial p}{\partial x}\right) + \frac{1}{A}\frac{\partial A}{\partial x}v + \frac{\partial v}{\partial x} = 0, \tag{24a}$$

$$\frac{1}{\rho}\frac{\partial p}{\partial x} + \left(\frac{\partial v}{\partial t} + v\frac{\partial v}{\partial x}\right) + \frac{\lambda v\,|v|}{2D} + g\sin(\alpha) = 0, \tag{24b}$$

where a is the wave speed, $A(x)$ is the cross sectional area, $D(x)$ the corresponding diameter, α the inclination of the pipe segment and λ the Darcy-Weissbach friction parameter. Table 3 summarizes the parameters of the hydraulic pipe system of the power plant. It is assumed that the diameter $D(x)$ of a pipe element varies linearly with the position x along the pipe, i.e. $D(x) = D(0)+(D(l)-D(0))x/l$, with the diameters $D(0)$ and $D(l)$ corresponding to the areas $A(0)$ and $A(l)$ at the beginning and the end of the pipe segment, respectively.

Table 3: Parameters of the pipe system according to Fig. 1.

i	$\frac{l_i}{l_{max}}$	$\frac{A_i(0)}{A_{max}}$	$\frac{A_i(l)}{A_{max}}$	α_i	a_i	$\lambda_i \times 1$
1	2.0×10^{-1}	1.00	1.00	$-3.7°$	1250 m/s	5.3
2	6.2×10^{-3}	1.00	0.85	$-3.7°$	1250 m/s	5.3
3	3.8×10^{-1}	0.85	0.85	$-90°$	1250 m/s	5.3
4	5.9×10^{-3}	0.85	0.43	$0°$	1200 m/s	5.3
5	9.7×10^{-2}	0.43	0.43	$0°$	1200 m/s	5.3
6	3.0×10^{-3}	0.21	0.23	$0°$	1200 m/s	5.8
7	2.7×10^{-2}	0.23	0.23	$0°$	1200 m/s	5.8
8	4.9×10^{-2}	0.32	0.32	$6.1°$	1250 m/s	5.8
9	3.1×10^{-3}	0.32	0.21	$6.1°$	1250 m/s	5.8
10	4.0×10^{-2}	0.43	0.43	$6.1°$	1250 m s	5.3
11	6.2×10^{-3}	0.43	1.00	$6.1°$	1250 m/s	5.3
12	1.0	1.00	1.00	$5.6°$	1250 m/s	5.3

The interconnection of the pipe segments and the connection with the pump turbine or the reservoirs is represented by suitable boundary conditions. Assuming that the filling levels of the reservoirs are approximately constant during the considered short time scales of the dynamics simulations, the upper and the lower reservoir introduce the following boundary conditions

$$p_1(0) = p_{UR} \quad \text{and} \quad p_{12}(l_{12}) = p_{LR}, \tag{25}$$

with the pressures p_{UR} and p_{LR} at the inlets of the upper and lower reservoir.

The lossless connection of two pipe segments i and $i+1$ with differing parameters is modeled by the boundary conditions

$$p_i(l_i, t) = p_{i+1}(0, t), \tag{26a}$$

$$q_i(l_i, t) = q_{i+1}(0, t), \tag{26b}$$

$i = 1, \ldots, 11$. The boundary conditions for a lossless junction of the pipe segment i into the two pipe segments

Post-print version of the article: J. Schmidt, W. Kemmetmüller, and A. Kugi, "Modeling and static optimization of a variable speed pumped storage power plant", *Renewable Energy*, vol. 111, pp. 38–51, 2017. DOI: https://dx.doi.org/10.1016/j.renene.2017.03.055
The content of this post-print version is identical to the published paper but without the publisher's final layout or copy editing.

j and k are given by

$$p_i(l_i,t) = p_j(0,t) = p_k(0,t), \tag{27a}$$
$$q_i(l_i,t) = q_j(0,t) + q_k(0,t), \tag{27b}$$

and the boundary conditions for the junction of pipe segments j and k to pipe segment i read as

$$p_i(0,t) = p_j(l_j,t) = p_k(l_k,t), \tag{28a}$$
$$q_i(0,t) = q_j(l_j,t) + q_k(l_k,t). \tag{28b}$$

Finally, the connection of a pump turbine to the upstream pipe segment i and the downstream pipe segment j is described by the boundary conditions

$$p_i(l_i,t) = p_j(0,t) + \Delta p_{PT} \tag{29a}$$
$$q_i(l_i,t) = q_j(0,t) = q_{PT}, \tag{29b}$$

where the pressure drop $\Delta p_{PT} = p_{US} - p_{DS}$ is defined as a function of the volume flow q_{PT}, the guide vane position χ and the rotary speed N of the pump turbine by

$$\Delta p_{PT} = \rho g \left(H_n - \Delta z - q_{PT}^2 \frac{\frac{1}{(A_i(l_i))^2} - \frac{1}{(A_j(0))^2}}{2g} \right), \tag{30}$$

cf. (19). Here, the net head $H_n = H_n(\chi, N, q_{PT})$ is defined by (23a).

In conclusion, the overall hydraulic part of the power plant is represented by a set of coupled PDEs, which needs to be numerically solved for a dynamic simulation of the power plant. For this task, it is useful to apply a number of simplifications to (24): (i) In the present application, the fluid velocity is much smaller than the wave speed, i.e. $v \ll a$, which allows to neglect the convective terms $v\frac{\partial p}{\partial x}$ and $v\frac{\partial v}{\partial x}$ in (24), see, e.g., [37]. (ii) It is further feasible to assume a constant mass density $\rho = 1000\,\mathrm{kg/m^3}$ and a constant wave speed[3] a. This yields a simplified PDE of the form

$$\frac{1}{\rho a^2}\frac{\partial p}{\partial t} + \frac{1}{A}\frac{\partial A}{\partial x} v + \frac{\partial v}{\partial x} = 0, \tag{31a}$$
$$\frac{1}{\rho}\frac{\partial p}{\partial x} + \frac{\partial v}{\partial t} + \frac{\lambda v\,|v|}{2D} + g\sin(\alpha) = 0, \tag{31b}$$

which can be numerically solved by applying the well-established MOC, see, e.g., [31]. To do so, the simplified PDE (31) is transformed to

$$\frac{\mathrm{d}p}{\mathrm{d}t} \pm \rho a \frac{\mathrm{d}v}{\mathrm{d}t} + \frac{\rho a^2}{A}\frac{\partial A}{\partial x} v \pm \rho a \left(\frac{\lambda v\,|v|}{2D} + g\sin(\alpha) \right) = 0, \tag{32}$$

which is defined on the characteristics

$$\frac{\mathrm{d}x}{\mathrm{d}t} = \pm a. \tag{33}$$

To solve this set of differential equations, a discretization in time and space is used in the subsequent simulations, see, e.g., [31].

[3] Note that the wave speed summarizes the effects of the fluid compressibility and the pipe wall elasticity.

2.3. Drive Train

The drive train couples the turbine with the generator and thus the hydraulic with the electric subsystem. Using the base quantities in Table 1, the balance of momentum for the drive train in per unit representation is given by

$$2\mathcal{H}\frac{\mathrm{d}\tilde{\omega}}{\mathrm{d}t} = \tilde{T} + \tilde{T}_{PT} - \tilde{d}_c\,\mathrm{sign}(\tilde{\omega}) - \tilde{d}_q\tilde{\omega}\,|\tilde{\omega}|\,, \tag{34}$$

with the inertia constant $\mathcal{H}$, see, e.g., [21], comprising the inertia of the pump turbine and the rotor of the DFIM. The torque $\tilde{T}$ of the DFIM and the torque $\tilde{T}_{PT}$ are given by (7) and the per unit representation of (23b), respectively. The mechanical losses of the drive train are split into a Coulomb part $\tilde{d}_c\,\mathrm{sign}(\tilde{\omega})$ and a quadratic part due to ventilation losses $\tilde{d}_q\tilde{\omega}\,|\tilde{\omega}|$. Table 4 summarizes the essential parameters of the mechanical system.

Table 4: Parameters of the mechanical system.

Parameter	Value	Unit
$\mathcal{H}$	3.86	s
$\tilde{d}_c$	4.12×10^{-3}	
$\tilde{d}_q$	6.13×10^{-3}	

3. Transient Simulation

As it is discussed in the introduction, the mathematical model developed in the previous section serves two purposes: (i) First, it is capable of accurately simulating the transient system behavior. Thus, it is suitable for an analysis of the dynamic system behavior and for testing different control and operating strategies in simulation studies. (ii) Second, the mathematical model also serves as a basis for reduced models, which are used for the design of control and estimation strategies. In this context, optimal operating and control strategies, which allow for energy-optimal (dynamic) operation of the power plant, are of particular interest.

In the next section, a simplified model is derived and optimal stationary operating points are calculated. In this section, some main features of the pumped storage power plant are discussed using transient simulations of the mathematical model. For this purpose, the model is implemented in Matlab/Simulink. The MOC is applied for the numerical solution of the PDEs of the pipe system, using a total of 594 spatial discretization points.

At first, it is assumed that both plant units A and B are operated identically. In the following simulation results, values of volume flow and pressure are depicted in per unit representation. Therefore, the base volume flow $q_b = q_{PT,r}$ and the base pressure $p_b = S_b/q_b$ are defined, see Table 5.

Fig. 4 depicts simulation results of the open-loop behavior of the power plant for filtered (first order delay with 100 ms rise time) step-like changes of the inputs $\mathbf{u}_e^{\mathrm{T}} =$

Post-print version of the article: J. Schmidt, W. Kemmetmüller, and A. Kugi, "Modeling and static optimization of a variable speed pumped storage power plant", *Renewable Energy*, vol. 111, pp. 38–51, 2017. DOI: https://dx.doi.org/10.1016/j.renene.2017.03.055
The content of this post-print version is identical to the published paper but without the publisher's final layout or copy editing.

Table 5: Base quantities of the hydraulic subsystem.

Parameter	Value	Unit
q_b	47.59	m^3/s
p_b	38.35	bar

$[\tilde{u}_{d2}^C, \tilde{u}_{q2}^C, \tilde{u}_{d2}^D, \tilde{u}_{q2}^D]$ of the electric system and χ of the hydraulic system. The input values in Fig. 4(a) correspond to stationary operating points with $P_{grid}^A = P_{grid}^B = 160\,\mathrm{MW}$ and $P_{grid}^A = P_{grid}^B = 55\,\mathrm{MW}$ active power, respectively, using a power factor of $\cos(\varphi) = 0.9$ to calculate the corresponding reactive power $Q_{grid}^A = Q_{grid}^B$.

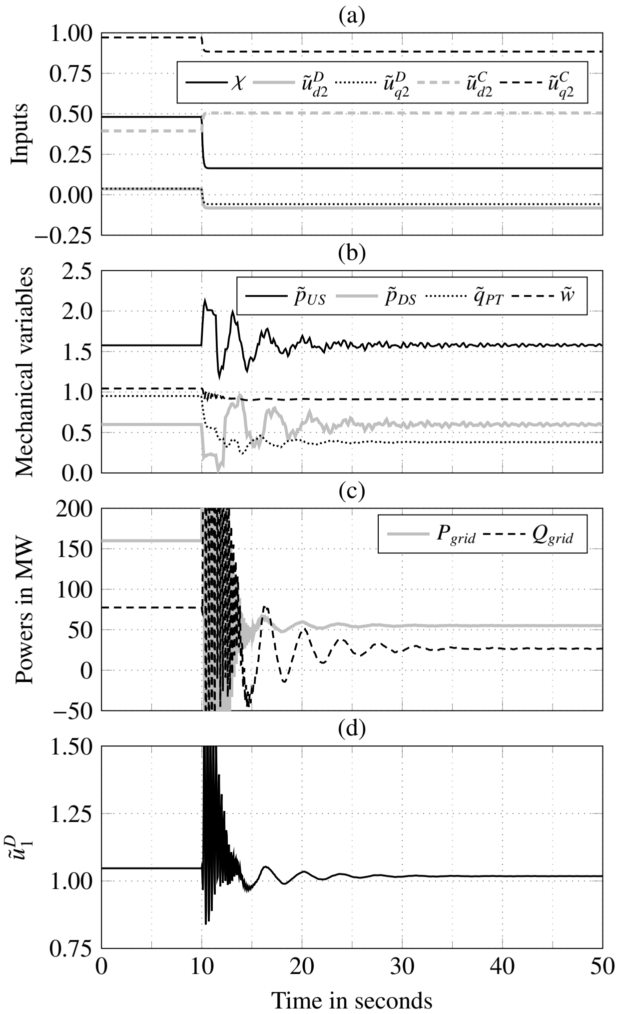

Figure 4: Fast change of operating points from $P_{grid}^A = P_{grid}^B = 160\,\mathrm{MW}$ to $P_{grid}^A = P_{grid}^B = 55\,\mathrm{MW}$: (a) System inputs, (b) mechanical system variables, (c) active and reactive power and (d) magnitude of the stator voltage $\tilde{u}_1^D$.

Fig. 4(b) shows the upstream pressure $\tilde{p}_{US} = \tilde{p}_7(l_7)$, the downstream pressure $\tilde{p}_{DS} = \tilde{p}_8(0)$, the volume flow $\tilde{q}_{PT}$ and the rotational speed $\tilde{\omega}$ of the pump turbine. The rapid reduction of the guide vane opening causes a fast decrease of the volume flow $\tilde{q}_{PT}$. Furthermore, large oscillations are induced in the upstream and downstream pressures, which propagate through the pipe system as pressure waves. The peak value of the upstream pressure exceeds the stationary pressure by almost 35%, which poses a possible threat to the pipe's mechanical integrity. A similar problem occurs for the downstream pressure which almost reaches zero. In this case, cavitation can occur, which also results in large stress of the pipe system and the turbine. These simulation results show that water hammer effects are immanent hazards to pumped storage power plants if fast changes between operating points occur.

In Fig. 4(c) the active and reactive output power of one plant unit are shown. The pronounced oscillating behavior after changing the operating point indicates a significantly faster dynamics of the electric system in comparison to the hydraulic and mechanical system. This fact can be advantageously used for the design of a control strategy, where, e.g., a cascaded control of the electric and hydraulic system is employed. Note that the oscillations in the electric system can be easily suppressed by a suitable control of the inverter of the DFIM. Finally, the magnitude of the stator voltage

$$\tilde{u}_1^D = \sqrt{\left(\tilde{u}_{d1}^D\right)^2 + \left(\tilde{u}_{q1}^D\right)^2} \tag{35}$$

is depicted in Fig. 4(d), which also shows large variations during the fast transition. Fig. 5 illustrates this transition in the pump turbine characteristic map.

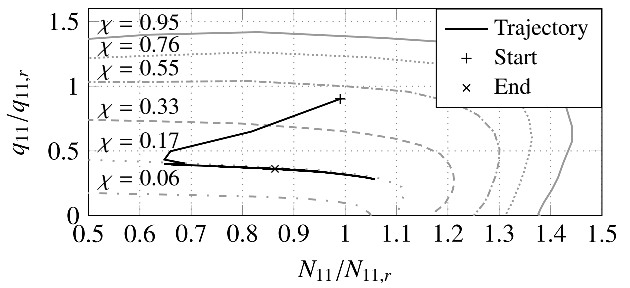

Figure 5: Fast change of operating points from $P_{grid}^A = P_{grid}^B = 160\,\mathrm{MW}$ to $P_{grid}^A = P_{grid}^B = 55\,\mathrm{MW}$: Trajectory in the pump turbine characteristics.

To point out the strong dynamic coupling between the plant units, the simulation is repeated applying the step-like changes in Fig. 4(a) only to unit A, while keeping the inputs of unit B constant. Fig. 6 reveals that the pressure waves initiated at pump turbine A travel along to pump turbine B, driving it away from its initial stationary operating point. At the end of the simulation horizon, the system is in a condition of slowly decaying oscillations. Apparently, in the case of independent operation, the plant units can cause remarkable mutual disturbances, which have to be thoroughly treated by a control strategy.

Large oscillations in the pressures and the active and reactive power are inadmissible in practical application and

Post-print version of the article: J. Schmidt, W. Kemmetmüller, and A. Kugi, "Modeling and static optimization of a variable speed pumped storage power plant", *Renewable Energy*, vol. 111, pp. 38–51, 2017. DOI: https://dx.doi.org/10.1016/j.renene.2017.03.055
The content of this post-print version is identical to the published paper but without the publisher's final layout or copy editing.

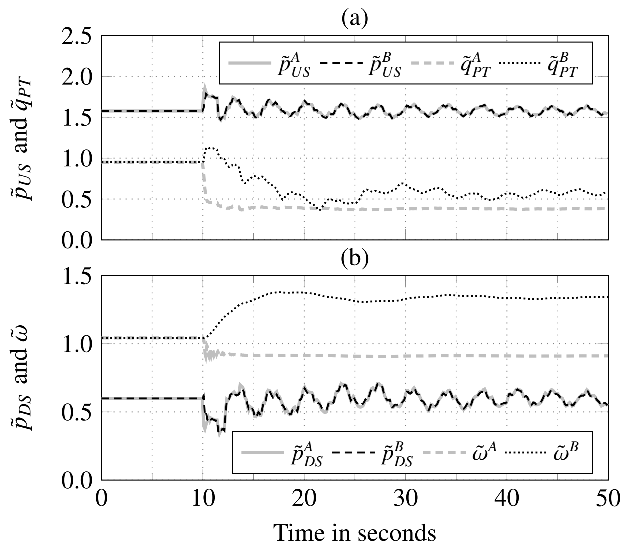

Figure 6: Fast change of operating points for independent operating plant units: (a) Upstream pump turbine pressure $\tilde{p}_{US}$ and pump turbine volume flow $\tilde{q}_{PT}$ of units A and B, (b) Downstream pump turbine pressure $\tilde{p}_{DS}$ and angular velocity $\tilde{\omega}$ of units A and B.

are prevented by limiting the rate of change of, e.g., the guide vane position χ in existing pumped storage power plants. This, on the other hand, also limits the rate of change of the output power, which is a major drawback if the power plant should be used for the stabilization of fast fluctuations in the grid. An accurate model which correctly predicts the water hammer phenomena in the pipe system, as the one presented in this paper, is thus indispensable for the design and test of control strategies which allow for a fast reaction to fluctuations in the distribution network.

4. Optimal Stationary Operating Points

The presented dynamical model can be used as the basis for dynamic simulation studies, the design of control and observer strategies and the calculation of optimal stationary and dynamic operating strategies. In this section, optimal stationary operating points are calculated for given values of the active and reactive power, P_{grid} and Q_{grid}, respectively, based on a minimization of the overall system losses. To do so, a stationary solution of the pipe system model is determined in the subsequent section. This stationary pipe model in combination with the stationary equations of the electric system serves as the basis for the formulation of the optimization problem to minimize the system losses.

4.1. Stationary Solution of the Pipe System

If the time derivative $\partial p/\partial t$ in (31a) is set to zero, it is immediately clear that the volume flow $q(x)$ is independent of x, i.e. $q(x) = q = \text{const.}$. Using this result and $\partial q/\partial t = 0$ in (31b), and integration over the pipe length l, gives the pressure drop $p(l) - p(0)$ over this pipe segment in the form

$$\begin{aligned} p(l) = p(0) - q(l)^2 \rho \frac{\frac{1}{(A(l))^2} - \frac{1}{(A(0))^2}}{2} \\ - q(l)\,|q(l)|\,\frac{\rho\lambda}{2}\int_0^l \frac{1}{D(x)\,(A(x))^2}\mathrm{d}x - \rho g l \sin(\alpha). \end{aligned} \tag{36}$$

Application of this stationary solution to the equations of the interconnected pipe system gives, after some calculations, the stationary solution of the overall pipe system in the form

$$\begin{aligned} 0 = \rho g(H_g - H_n(\chi^A, N^A, q^A_{PT})) + \left(q^A_{PT}\right)^2 c_0 \\ - \left(q^A_{PT} + q^B_{PT}\right)\left|q^A_{PT} + q^B_{PT}\right| c_1 - q^A_{PT}\left|q^A_{PT}\right| c_2 \end{aligned} \tag{37a}$$

$$\begin{aligned} 0 = \rho g(H_g - H_n(\chi^B, N^B, q^B_{PT})) + \left(q^B_{PT}\right)^2 c_0 \\ - \left(q^A_{PT} + q^B_{PT}\right)\left|q^A_{PT} + q^B_{PT}\right| c_1 - q^B_{PT}\left|q^B_{PT}\right| c_2, \end{aligned} \tag{37b}$$

where A and B refer to the two pump turbines of the pumped storage power plant. The overall gross head H_g is given by

$$H_g = \frac{p_{UR} - p_{LR}}{\rho g} + \Delta z - \sum_{i=1}^{12} l_i \sin(\alpha_i)$$

and the coefficients $c_0, \ldots, c_2$ in (37) are defined as

$$\begin{aligned} c_0 &= \frac{\rho}{2}\left(\left(\frac{1}{A_{US}}\right)^2 - \left(\frac{1}{A_{DS}}\right)^2\right) \\ c_1 &= \frac{\rho}{2}\sum_{i \in I_c}\lambda_i \int_0^{l_i} \frac{1}{D_i(x)\,(A_i(x))^2}\mathrm{d}x \\ c_2 &= \frac{\rho}{2}\sum_{i \in I_b}\lambda_i \int_0^{l_i} \frac{1}{D_i(x)\,(A_i(x))^2}\mathrm{d}x. \end{aligned}$$

Therein, the set I_c refers to the pipes which are common to both pump turbine units, $I_c = \{1, \ldots, 5, 10, \ldots, 12\}$ and I_b summarizes the branched pipe segments, i.e., $I_b = \{6, \ldots, 9\}$.

The hydraulic input power for the turbine operation is defined as

$$P_{hyd,in} = \rho g \left(q^A_{PT} + q^B_{PT}\right) H_g + \left(\left(q^A_{PT}\right)^3 + \left(q^B_{PT}\right)^3\right) c_0. \tag{39}$$

Utilizing the stationary solution (37), the balance of hydraulic power can be formulated as $P_{hyd,in} = P^A_{in} + P^B_{in} + P_{diss}$, with the hydraulic input power P^A_{in} and P^B_{in} of pump turbine A and B, respectively, and the dissipated power

Post-print version of the article: J. Schmidt, W. Kemmetmüller, and A. Kugi, "Modeling and static optimization of a variable speed pumped storage power plant", *Renewable Energy*, vol. 111, pp. 38–51, 2017. DOI: https://dx.doi.org/10.1016/j.renene.2017.03.055
The content of this post-print version is identical to the published paper but without the publisher's final layout or copy editing.

P_{diss} due to the friction in the pipe system.

$$P_{in}^{A} = \rho g q_{PT}^{A} H_n\left(\chi^A, N^A, q_{PT}^{A}\right) \tag{40a}$$
$$P_{in}^{B} = \rho g q_{PT}^{B} H_n\left(\chi^B, N^B, q_{PT}^{B}\right) \tag{40b}$$
$$P_{diss} = (q_{PT}^{A} + q_{PT}^{B})^2 |q_{PT}^{A} + q_{PT}^{B}| c_1 + \left(\left(q_{PT}^{A}\right)^2 \left|q_{PT}^{A}\right| + \left(q_{PT}^{B}\right)^2 \left|q_{PT}^{B}\right|\right) c_2 \tag{40c}$$

4.2. Constrained Nonlinear Optimization Problem

In this section, optimal stationary operating points for the pumped storage power plant comprising two pump turbines, which share a common pipe system, are calculated. The main goal is to minimize the losses P_l of the overall hydraulic and electric system. The stationary system losses consist of

- pipe friction losses,
- hydraulic losses in the pump turbines,
- mechanical friction and ventilation losses and
- electric losses including losses of the VSCs as well as copper and iron losses of the converter transformers and the DFIMs.

A per unit representation of the complete system is applied for the numerical treatment of the optimization problem, using the respective base quantities, see Tables 1 and 5.

Instead of summarizing all the individual losses, the overall losses can be formulated as the difference of the hydraulic input power $\tilde{P}_{hyd,in}$ and the power supplied to the distribution network $\tilde{P}_{grid}^{A} + \tilde{P}_{grid}^{B}$, i.e.

$$\tilde{P}_l(\mathbf{x}, \mathbf{u}) = \tilde{P}_{hyd,in} - \tilde{P}_{grid}^{A} - \tilde{P}_{grid}^{B}. \tag{41}$$

Therein, the input and output power are (nonlinear) functions of the system state $\mathbf{x}$ and system input $\mathbf{u}$

$$\mathbf{x}^{\mathrm{T}} = \begin{bmatrix} \tilde{q}_{PT}^{A} & \tilde{\omega}^{A} & \left(\mathbf{x}_e^{A}\right)^{\mathrm{T}} & \tilde{q}_{PT}^{B} & \tilde{\omega}^{B} & \left(\mathbf{x}_e^{B}\right)^{\mathrm{T}} \end{bmatrix} \tag{42a}$$
$$\mathbf{u}^{\mathrm{T}} = \begin{bmatrix} \chi^{A} & \left(\mathbf{u}_e^{A}\right)^{\mathrm{T}} & \chi^{B} & \left(\mathbf{u}_e^{B}\right)^{\mathrm{T}} \end{bmatrix}. \tag{42b}$$

In addition to minimizing the overall system losses, the stationary operating points should be calculated such that the active and reactive power $\tilde{P}_{grid}^{j}$ and $\tilde{Q}_{grid}^{j}$, $j \in \{A, B\}$, supplied to the grid by the two DFIMs are equal to the desired values $\tilde{P}_{grid}^{j*}$ and $\tilde{Q}_{grid}^{j*}$. This is considered in the optimization task by the equality constraints

$$g_1^j(\mathbf{x}, \mathbf{u}) = \tilde{P}_{grid}^{j} - \tilde{P}_{grid}^{j*} = 0 \tag{43a}$$
$$g_2^j(\mathbf{x}, \mathbf{u}) = \tilde{Q}_{grid}^{j} - \tilde{Q}_{grid}^{j*} = 0, \tag{43b}$$

$j \in \{A, B\}$. Furthermore, in order to reduce the losses of the grid side inverter, it is common practice to set the reactive power $\tilde{Q}_1^{Cj}$ at the converter transformers to zero, i.e.

$$g_3^j(\mathbf{x}, \mathbf{u}) = \tilde{u}_{q1}^{Cj} \tilde{i}_{d1}^{Cj} - \tilde{u}_{d1}^{Cj} \tilde{i}_{q1}^{Cj} = 0, \quad j \in \{A, B\}. \tag{43c}$$

Finally, a stationary operating point is obtained by (37) and by setting the right hand sides of (15) and (34) to zero.

For a stationary operating point to be feasible, the constraints of the real system have to be met. The guide vane position χ^j is limited by $\chi_{min} \leq \chi^j \leq \chi_{max}$, which can be equivalently formulated by

$$h_1^j(\mathbf{x}, \mathbf{u}) = \chi^j - \chi_{max} \leq 0 \tag{44a}$$
$$h_2^j(\mathbf{x}, \mathbf{u}) = -\chi^j + \chi_{min} \leq 0, \tag{44b}$$

for $j \in \{A, B\}$. The stator and rotor current amplitudes of the DFIM are limited due to thermal constraints in the form

$$h_3^j(\mathbf{x}, \mathbf{u}) = \left(\tilde{i}_{d1}^{Dj}\right)^2 + \left(\tilde{i}_{q1}^{Dj}\right)^2 - \left(\tilde{i}_{1,max}^{Dj}\right)^2 \leq 0 \tag{44c}$$
$$h_4^j(\mathbf{x}, \mathbf{u}) = \left(\tilde{i}_{d2}^{Dj}\right)^2 + \left(\tilde{i}_{q2}^{Dj}\right)^2 - \left(\tilde{i}_{2,max}^{Dj}\right)^2 \leq 0 \tag{44d}$$

and the rotor voltage amplitude is basically limited by the DC voltage of the VSC

$$h_5^j(\mathbf{x}, \mathbf{u}) = \left(\tilde{u}_{d2}^{Dj}\right)^2 + \left(\tilde{u}_{q2}^{Dj}\right)^2 - \left(\tilde{u}_{2,max}^{Dj}\right)^2 \leq 0, \tag{44e}$$

$j \in \{A, B\}$. Finally, the rotor active power is limited due to the thermal constraints of the VSC by

$$h_6^j(\mathbf{x}, \mathbf{u}) = \tilde{u}_{d2}^{Dj} \tilde{i}_{d2}^{Dj} + \tilde{u}_{q2}^{Dj} \tilde{i}_{q2}^{Dj} - \tilde{P}_{2,max}^{D} \leq 0 \tag{44f}$$
$$h_7^j(\mathbf{x}, \mathbf{u}) = -\tilde{u}_{d2}^{Dj} \tilde{i}_{d2}^{Dj} - \tilde{u}_{q2}^{Dj} \tilde{i}_{q2}^{Dj} - \tilde{P}_{2,max}^{D} \leq 0. \tag{44g}$$

The respective limits are summarized in Table 6.

Table 6: Limits for the inequality constraints (44).

Parameter	Value
χ_{min}	0.06
χ_{max}	0.95
$\tilde{P}_{2,max}^{D}$	0.082
$\tilde{i}_{1,max}^{D}$	1.000
$\tilde{i}_{2,max}^{D}$	1.346
$\tilde{u}_{2,max}^{D}$	0.121

In order to avoid results outside of valid area of the interpolated pump turbine characteristic maps, cf. Fig. 3, the auxiliary inequality constraints

$$h_8^j(\mathbf{x}, \mathbf{u}) = \tilde{P}_{out}^{j} - \tilde{P}_{in}^{j} \leq 0, \tag{45}$$

$j \in \{A, B\}$, are introduced. Therein $\tilde{P}_{out}^{j} = \tilde{\omega}^j \tilde{T}_{PT}^{j}$ and $\tilde{P}_{in}^{j}$ represent the per unit mechanical output power and the per unit hydraulic input power, cf. (40a) and (40b), of the respective pump turbines.

Putting together the equality and inequality constraints, the task of calculating optimal stationary operating points

Post-print version of the article: J. Schmidt, W. Kemmetmüller, and A. Kugi, "Modeling and static optimization of a variable speed pumped storage power plant", *Renewable Energy*, vol. 111, pp. 38–51, 2017. DOI: https://dx.doi.org/10.1016/j.renene.2017.03.055
The content of this post-print version is identical to the published paper but without the publisher's final layout or copy editing.

is formulated as the constrained nonlinear optimization problem

$$\begin{aligned} \min_{\mathbf{u}} \quad & \tilde{P}_l(\mathbf{x}, \mathbf{u}) \\ \text{s.t.} \quad & \mathbf{g}(\mathbf{x}, \mathbf{u}) = \mathbf{0} \\ & \mathbf{h}(\mathbf{x}, \mathbf{u}) \leq \mathbf{0}. \end{aligned} \tag{46}$$

This optimization problem is numerically solved by a gradient based method using the `fmincon` command of MATLAB. The utilization of a B-Spline interpolation of the pump turbine characteristics of Fig. 3 allows to provide analytical expressions for all required gradients, which significantly improves the accuracy and speed of the numerical solution.

In the following, optimal stationary operating points are presented for four scenarios: (i) In the first scenario, both plant units are operated identically, i.e. with the same inputs, states and output power, which is a possible operating mode when the two plant units are owned by one company. (ii) For small values of the desired grid power, the results of (i) are compared with the optimal operation using only a single plant unit, while the other plant unit is switched off. (iii) Typically, both plant units distribute their power to the same transmission line. Thus, the third operating scenario examines if there are any benefits of a coordinated operation of the two plant units. (iv) Finally, the advantages of a variable speed system in view of the overall efficiency of the plant and the operating range is examined in the fourth scenario.

It has to be noted that the optimal operating points are strongly influenced by the interpolated characteristic maps $W_H(\chi, \theta)$ and $W_B(\chi, \theta)$, cf. Fig. 3. Therefore, the reliability of the optimization results strongly depends on the accuracy of the pump turbine characteristics.

4.3. Identical Operation of Plant Units

In this first scenario, it is assumed that both plant units are operated identically in turbine mode, distributing the same active power $P^A_{grid} = P^B_{grid}$ to the grid. A series of 200 optimal stationary operating points is calculated for three different gross heads $H_g = 275\,\text{m}$, $H_g = 335\,\text{m}$ and $H_g = 395\,\text{m}$. Here, the first value corresponds to the minimum gross head for almost empty upper reservoir and almost completely filled lower reservoir, while the last value is given for an almost completely filled upper reservoir and almost empty lower reservoir. The range of the desired active power P^*_{grid} delivered to the distribution network is then defined in the form

$$\begin{aligned} P^*_{grid} &= 100\,\text{MW}, \ldots, 250\,\text{MW} \quad \text{for} \quad H_g = 275\,\text{m} \\ P^*_{grid} &= 100\,\text{MW}, \ldots, 340\,\text{MW} \quad \text{for} \quad H_g = 335\,\text{m} \\ P^*_{grid} &= 100\,\text{MW}, \ldots, 350\,\text{MW} \quad \text{for} \quad H_g = 395\,\text{m}, \end{aligned}$$

with $P^*_{grid} = P^{A*}_{grid} + P^{B*}_{grid}$. The desired reactive power $Q^*_{grid} = Q^{A*}_{grid} + Q^{B*}_{grid} > 0$ is set according to the power

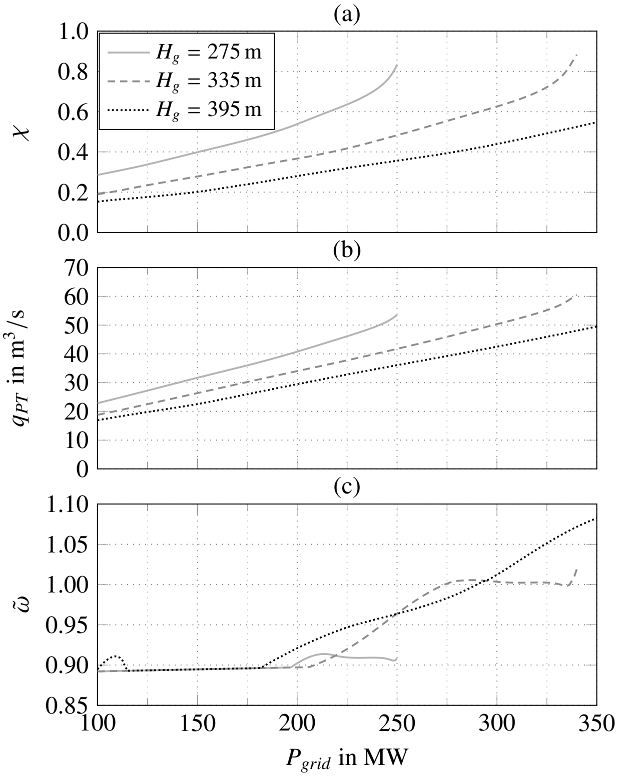

Figure 7: Optimal stationary operating points for identical operation of the plant units: (a) guide vane opening χ, (b) volume flow of a plant unit q_{PT} and (c) angular velocity $\tilde{\omega}$.

factor $\cos(\varphi) = 0.9$, which is the equivalent choice as has been used in the dynamic simulations in Section 3.

The resulting values of the guide vane position χ, the volume flow q_{PT} and angular velocity $\tilde{\omega}$ are depicted in Fig. 7. Fig. 7(b) reveals that smaller gross heads H_g imply higher volume flows in order to produce the same hydraulic input power, cf. (39). This in turn leads to larger guide vane openings, as depicted in Fig. 7(a). Fig. 7(c) shows that the angular velocity of the plant units is generally decreased for lower desired grid power. The minimum velocity is, however, limited by the constraints of the electric system described in (44c)-(44g), in particular by the maximum rotor voltage which can be supplied by the VSI, see also Fig. 9(b).

The overall system efficiency for the turbine mode

$$\eta = \frac{\tilde{P}^A_{grid} + \tilde{P}^B_{grid}}{\tilde{P}_{hyd,in}} \tag{48}$$

is depicted in Fig. 8(a), showing differing points of maximum efficiency for the three values of the gross head H_g. For all cases, however, a high overall system efficiency is obtained in a rather wide operating range of the desired grid power. To a significant degree, this can be attributed to the variable speed operation of the plants, which, in the case of $H_g = 335\,\text{m}$, will be shown in Section 4.5. The

Post-print version of the article: J. Schmidt, W. Kemmetmüller, and A. Kugi, "Modeling and static optimization of a variable speed pumped storage power plant", *Renewable Energy*, vol. 111, pp. 38–51, 2017. DOI: https://dx.doi.org/10.1016/j.renene.2017.03.055
The content of this post-print version is identical to the published paper but without the publisher's final layout or copy editing.

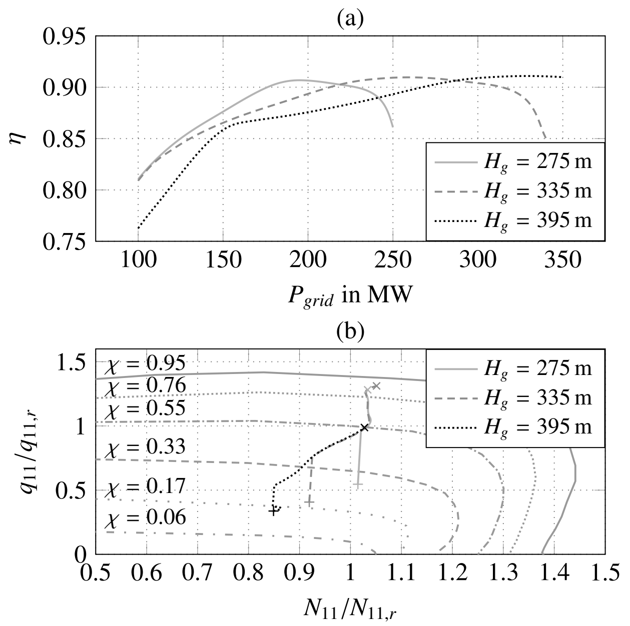

Figure 8: Optimal stationary operating points for identical operation of the plant units: (a) overall efficiency η and (b) operating points in the pump turbine characteristics.

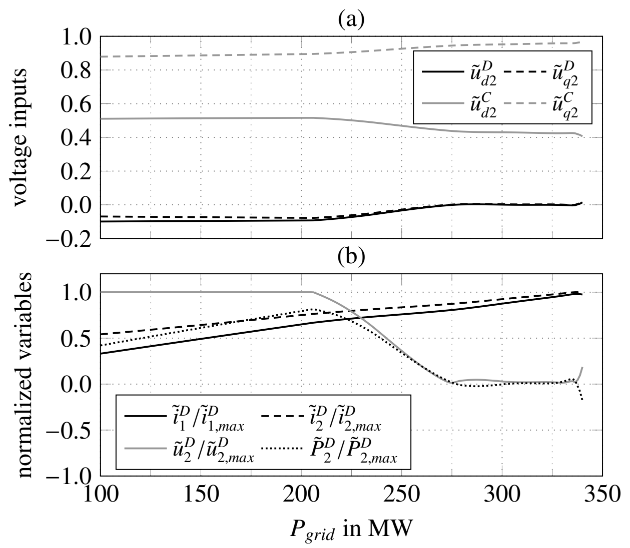

Figure 9: Optimal stationary operating points for identical operation of the plant units and $H_g = 335\,\text{m}$: (a) electric system inputs and (b) constrained electric variables.

operating points are represented in the characteristic map of the Francis turbine in Fig. 8(b), where again the operating area with constant angular velocity can be clearly identified.

Fig. 9(a) displays the electric system inputs, i.e. the rotor voltages $\tilde{u}^D_{d2}$, $\tilde{u}^D_{q2}$ and the grid side converter voltages $\tilde{u}^C_{d2}$, $\tilde{u}^C_{q2}$, necessary to obtain the desired grid power for the case $H_g = 335\,\text{m}$. In Fig. 9(b), the corresponding constrained variables of the electric system are shown. As already mentioned before, the magnitude $\tilde{u}^D_2$ of the rotor voltage sticks to its upper bound for $P_{grid} < 206\,\text{MW}$ resulting in the limitation of the angular velocity in Fig. 7(c).

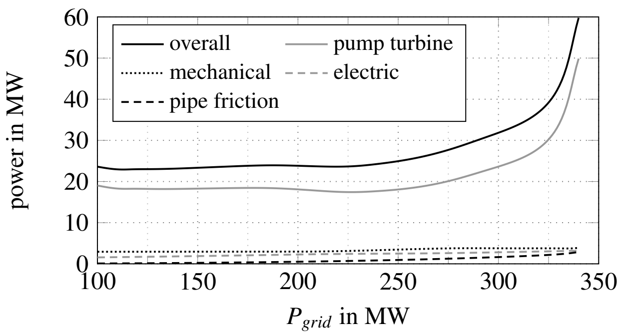

Figure 10: Optimal stationary operating points for identical operation of the plant units and $H_g = 335\,\text{m}$: analysis of the system losses.

Finally, Fig. 10 shows the contribution of the different parts of the plant to the overall system losses. Obviously, the majority of the system losses results from the losses in the pump turbine. On the other hand, with an overall amount of approximately 10 MW, consideration of the remaining losses (mechanical, electric and pipe friction losses) is certainly important and relevant for the calculation of optimal operating points.

4.4. Independent Operation and Single Plant Unit

In the last subsection, it was assumed that both plant units operate identically. The purpose of this subsection is to analyze if an improvement of the overall system efficiency can be achieved by an independent operation of the two plant units, which means that the assumption $P^{A*}_{grid} = P^{B*}_{grid}$ is dropped in the calculation of optimal operating points. Moreover, it is examined in which cases it is more efficient to operate only a single plant unit and to switch off the second plant unit. The subsequent optimization results are calculated for $H_g = 335\,\text{m}$, and the entire possible pumping and turbine mode of operation is considered. The corresponding maximum and minimum values of the grid power P^*_{grid} are limited by the system constraints. The desired reactive power $Q^*_{grid} > 0$ is again set according to the power factor $\cos(\varphi) = 0.9$.

Fig. 11(d) reveals that there is some room of improvements in terms of overall efficiency in the case of independent operation compared to the identical operation of the plant units, in particular for the pumping mode. These improvements of efficiency primarily result from reductions in pump turbine losses caused by asymmetric operating points, cf. Fig. 11(a)-(c). A larger share of the total power is transmitted over a pump turbine unit that is operated at higher efficiency. Furthermore, Fig. 11(d) shows that it is far more efficient to use a single plant unit for small values of the grid power P_{grid}, up to cases of almost

Post-print version of the article: J. Schmidt, W. Kemmetmüller, and A. Kugi, "Modeling and static optimization of a variable speed pumped storage power plant", *Renewable Energy*, vol. 111, pp. 38–51, 2017. DOI: https://dx.doi.org/10.1016/j.renene.2017.03.055
The content of this post-print version is identical to the published paper but without the publisher's final layout or copy editing.

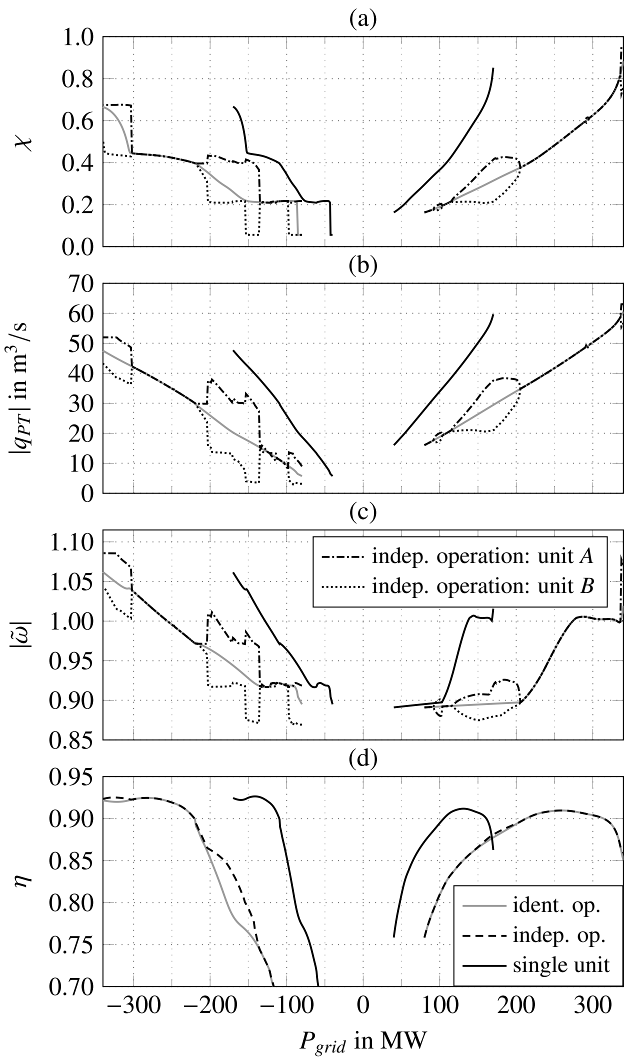

Figure 11: Optimal stationary operating points for independent operation of the plant units and single plant unit: (a) guide vane opening χ, (b) volume flow of a single plant unit q_{PT}, (c) angular velocity $\tilde{\omega}$ and (d) system efficiency η.

the maximum possible grid power of a single plant unit. This results from the fact that the dominating part of the overall system losses are the pump turbine losses, such that it makes sense to choose operating points of the plant where the efficiency of the pump turbine is best. Given the results of Fig. 11(d) this is the case for large values of the guide vane opening.

4.5. Variable and Fixed Angular Speed Operation

In this final simulation scenario, the benefits of a variable angular speed operation compared to an operation with fixed angular speed with respect to the overall system efficiency is examined. For this scenario, again an identical operation of both plant units is considered.

Fig. 12(a) shows that the overall system efficiency can be significantly increased by the variation of the angular speed of the pump turbine, in particular in operating ranges with a power below the rated power of the plant. Moreover, the overall feasible operating range of the pump turbine is increased by variable speed operation, which is most visible in the pumping mode of the power plant. Fig. 12(b) and 12(c) show the operating points in the characteristic map of the pump turbine.

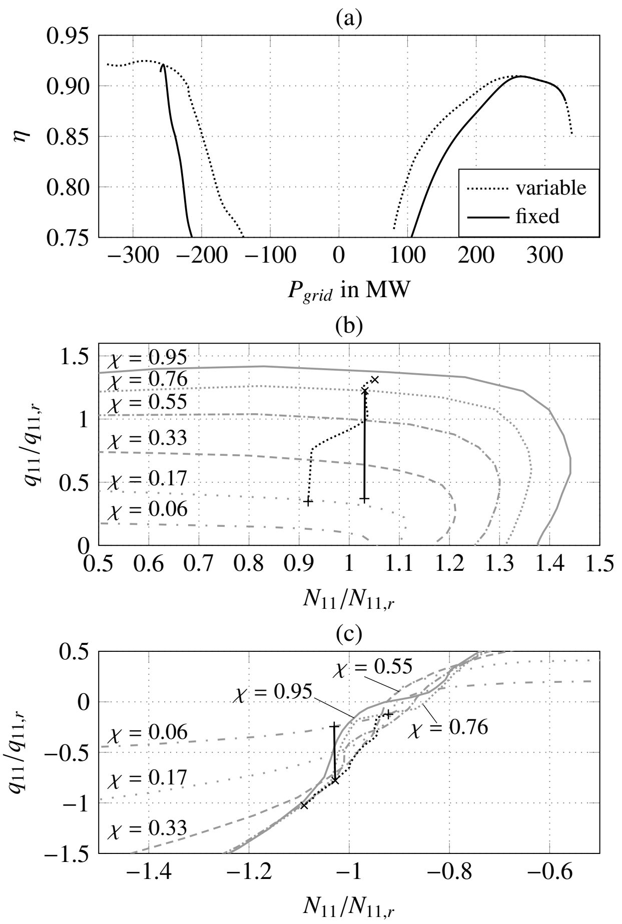

Figure 12: Optimal stationary operating points for variable and fixed angular speed operation: (a) overall system efficiency η, (b) and (c) operating points in the characteristic map of the pump turbine.

Finally, Fig. 13 shows the values of the guide vane position, the volume flow of a single plant unit and the angular speed corresponding to the optimal operating points. It can be deduced from these plots that in the pump mode more water can be pumped from lower reservoir to the upper by the variable speed plant compared to a fixed speed plant, while using the same electric input power. Analogously, less water is necessary to generate the same power using a variable speed plant compared to a fixed speed plant. These results clearly show the advantages of using a variable speed pumped storage plant system.

Post-print version of the article: J. Schmidt, W. Kemmetmüller, and A. Kugi, "Modeling and static optimization of a variable speed pumped storage power plant", *Renewable Energy*, vol. 111, pp. 38–51, 2017. DOI: https://dx.doi.org/10.1016/j.renene.2017.03.055
The content of this post-print version is identical to the published paper but without the publisher's final layout or copy editing.

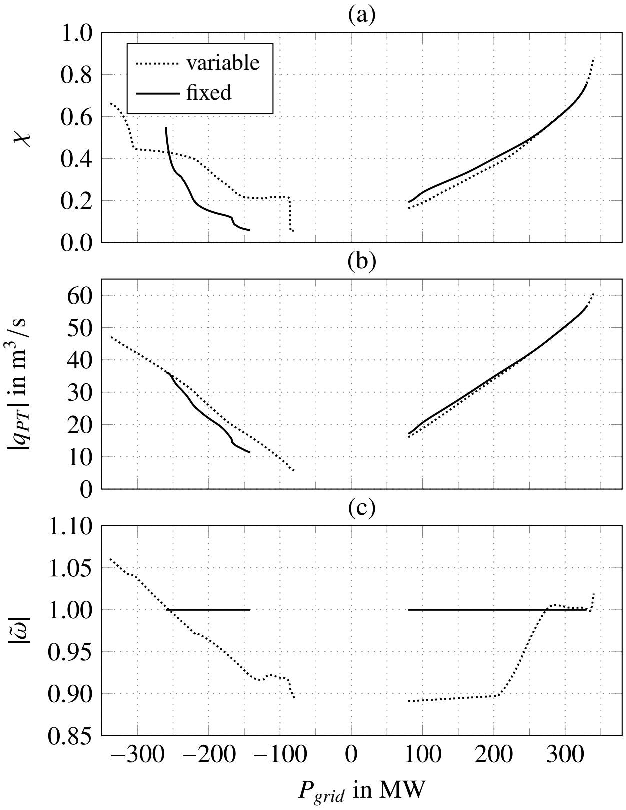

Figure 13: Optimal stationary operating points for variable and fixed angular speed operation: (a) guide vane opening χ, (b) volume flow of single plant unit q_{PT} and (c) angular speed $\tilde{\omega}$.

5. Conclusions

In this contribution, a detailed mathematical model of a variable speed pumped storage power plant is presented. The behavior of the electric and mechanical key components are considered to obtain a comprehensive description of the overall dynamic system behavior. In particular, the infinite-dimensional nature of the pipe system is properly handled by the application of the Method of Characteristics, accurately reproducing important dynamical effects like wave propagation due to water hammer. This mathematical model can therefore serve as a basis for dynamical simulation studies and the development and test of (optimal) control strategies.

The proposed model is also utilized to calculate optimal stationary operating points of minimum energy losses. The most important energy losses including pump turbine losses, pipe friction, mechanical friction as well as several electric losses are systematically included in the model. The nonlinear optimization problem also takes into account the constraints of the system states. Optimization results for different operating scenarios are presented, which clearly show the advantages of a variable speed plant compared to a fixed speed plant. Moreover, some important conclusions on the optimal operation of variable speed pumped storage power plants with double fed induction machines are drawn from these optimization results.

Acknowledgements

This research was funded by the Austrian Research Promotion Agency (FFG) under grant agreement numbers 833955 and 849267. The authors are grateful to the industrial research partner Andritz Hydro GmbH.

References

[1] J. I. Pérez-Díaz, M. Chazarra, J. García-González, G. Cavazzini, A. Stoppato, Trends and challenges in the operation of pumped-storage hydropower plants, Renewable and Sustainable Energy Reviews 44 (2015) 767–784.
[2] A. Hodder, Double-fed asynchronous motor-generator equipped with a 3-level VSI cascade, Ph.D. thesis, EPFL, Lausanne, Switzerland (2004).
[3] Y. Pannatier, Optimisation des stratégies de réglage d'une installation de pompage-turbinage à vitesse variable, Ph.D. thesis, EPFL, Lausanne, Switzerland (2010).
[4] Y. Pannatier, B. Kawkabani, C. Nicolet, J. J. Simond, A. Schwery, P. Allenbach, Investigation of Control Strategies for Variable-Speed Pump-Turbine Units by Using a Simplified Model of the Converters, IEEE Transactions on Industrial Electronics 57 (9) (2010) 3039–3049.
[5] E. Schmidt, J. Ertl, A. Preiss, R. Zensch, R. Schürhuber, J. Hell, Studies about the Low Voltage Ride Through Capabilities of Variable-Speedpeed Motor-Generators of Pumped Storage Hydro Power Plants, in: 21st Australasian Universities Power Engineering Conference (AUPEC), 2011, pp. 1–6.
[6] J. A. Suul, K. Uhlen, T. Undeland, et al., Variable speed pumped storage hydropower for integration of wind energy in isolated grids: case description and control strategies, in: Nordic Workshop on Power and Industrial Electronics (NORPIE), Espoo, Finland, 2008.
[7] P. Steimer, O. Senturk, S. Aubert, S. Linder, Converter-Fed Synchronous Machine for Pumped Hydro Storage Plants, in: Energy Conversion Congress and Exposition (ECCE), IEEE, Pittsburgh, PA, USA, 2014, pp. 4561–4567.
[8] H. Schlunegger, A. Thöni, 100 MW full-size converter in the Grimsel 2 pumped-storage plant, in: Hydro 2013, Innsbruck, Austria, 2013.
[9] A. Bocquel, J. Janning, Analysis of a 300 MW Variable Speed Drive for Pump-Storage Plant Applications, in: European Conference on Power Electronics and Applications, Dresden, Germany, 2005, pp. 1–10.
[10] J. Lung, Y. Lu, W. Hung, W. Kao, Modeling and Dynamic Simulations of Doubly Fed Adjustable-Speed Pumped Storage Units, IEEE Transactions on Energy Conversion 22 (2) (2007) 250–258.
[11] N. Sivakumar, D. Das, N. Padhy, Variable speed operation of reversible pump-turbines at Kadamparai pumped storage plant - A case study, Energy Conversion and Management 78 (2014) 96 – 104.
[12] J. Liang, R. G. Harley, Pumped Storage Hydro-Plant Models for System Transient and Long-Term Dynamic Studies, in: IEEE PES General Meeting, 2010, pp. 1–8.
[13] J. I. Sarasúa, J. I. Pérez-Díaz, J. R. Wilhelmi, J. Á. Sánchez-Fernández, Dynamic response and governor tuning of a long penstock pumped-storage hydropower plant equipped with a pump-turbine and a doubly fed induction generator, Energy Conversion and Management 106 (2015) 151–164.
[14] H. M. Gao, C. Wang, A Detailed Pumped Storage Station Model for Power System Analysis, in: IEEE Power Engineering Society General Meeting, 2006, pp. 1 – 5.

Post-print version of the article: J. Schmidt, W. Kemmetmüller, and A. Kugi, "Modeling and static optimization of a variable speed pumped storage power plant", *Renewable Energy*, vol. 111, pp. 38–51, 2017. DOI: https://dx.doi.org/10.1016/j.renene.2017.03.055
The content of this post-print version is identical to the published paper but without the publisher's final layout or copy editing.

[15] C. Nicolet, F. Avellan, P. Allenbach, A. Sapin, J.-J. Simond, New tool for the simulation of transient phenomena in Francis turbine power plants, in: IAHR Symposium, Lausanne, Switzerland, 2002.

[16] C. Nicolet, Hydroacoustic modelling and numerical simulation of unsteady operation of hydroelectric systems, Ph.D. thesis, EPFL, Lausanne, Switzerland (2007).

[17] W. Zeng, J. Yang, R. Tang, W. Yang, Extreme water-hammer pressure during one-after-another load shedding in pumped-storage stations, Renewable Energy 99 (2016) 35 – 44.

[18] J. Yang, J. Yang, B-spline surface construction for the complete characteristics of pump-turbine, in: 2012 Asia-Pacific Power and Energy Engineering Conference, 2012, pp. 1–5.

[19] Y. Liu, J. Yang, J. Yang, C. Wang, W. Zeng, Transient Simulations in Hydropower Stations Based on a Novel Turbine Boundary, Mathematical Problems in Engineering 2016, Article ID 1504659, 13 pages.

[20] C. Nicolet, E. F. R. Bollaert, P. Allenbach, A. Gal, Optimizing hydro production with a detailed simulation model, Hydropower & Dams 5 (2009) 77–81.

[21] P. Krause, O. Wasynczuk, S. Sudhoff, Analysis of Electric Machinery and Drive Systems, 2nd Edition, IEEE Press, Piscataway, New Jersey, USA, 2002.

[22] F. Bonnet, L. Lowinsky, M. Pietrzak-David, P.-É. Vidal, Doubly Fed Induction Machine Speed Drive for Hydro-Electric Power Station, in: European Conference on Power Electronics and Applications, Aalborg, Denmark, 2007, pp. 1–9.

[23] Y. Pannatier, B. Kawkabani, C. Nicolet, A. Schwery, J.-J. Simond, Start-up and Synchronization of a Variable Speed Pump-Turbine Unit in Pumping Mode, in: 19th International Conference on Electrical Machines (ICEM), Rome, Italy, 2010, pp. 1–6.

[24] A. Damdoum, I. Slama-Belkhodja, M. Pietrzak-David, M. Debbou, Low voltage ride-through strategies for doubly fed induction machine pumped storage system under grid faults, Renewable Energy 95 (2016) 248 – 262.

[25] E. Levi, Impact of Iron Loss on Behavior of Vector Vontrolled Induction Machines, IEEE Transactions on Industry Applications 31 (6) (1995) 1287–1296.

[26] S.-D. Wee, M.-H. Shin, D.-S. Hyun, Stator-Flux-Oriented Control of Induction Motor Considering Iron Loss, IEEE Transactions on Industrial Electronics 48 (3) (2001) 602–608.

[27] B. R. Oswald, Berechnung von Drehstromnetzen, Springer Vieweg, Wiesbaden, Germany, 2013.

[28] S. Kouro, J. Rodriguez, B. Wu, S. Bernet, M. Perez, Powering the future of industry: High-power adjustable speed drive topologies, Industry Applications Magazine, IEEE 18 (4) (2012) 26–39.

[29] W. Qiao, Dynamic Modeling and Control of Doubly Fed Induction Generators Driven by Wind Turbines, in: Power Systems Conference and Exposition, IEEE PES, Seattle, WA, USA, 2009, pp. 1–8.

[30] S. Dieckerhoff, S. Bernet, D. Krug, Power Loss-Oriented Evaluation of High Voltage IGBTs and Multilevel Converters in Transformerless Traction Applications, IEEE Trans. Power Electronics 20 (6) (2005) 1328–1336.

[31] E. B. Wylie, V. L. Streeter, Fluid Transients in Systems, Prentice-Hall, Englewood Cliffs, New Jersey, USA, 1993.

[32] R. Knapp, Complete Characteristics of Centrifugal Pumps and Their Use in the Prediction of Transient Behavior, Trans. ASME (1937) 683–689.

[33] N. Walmsley, The numerical representation of pump-turbine performance characteristics, Ph.D. thesis, University of Warwick, UK (1986).

[34] L. Piegl, W. Tiller, The Nurbs Book, Springer Berlin Heidelberg, New York, 1995.

[35] A. Adamkowski, Analysis of Transient Flow in Pipes With Expanding or Contracting Sections, Journal of fluids engineering 125 (4) (2003) 716–722.

[36] T. Wu, C.-C. Ferng, Effect of nonuniform conduit section on waterhammer, Acta Mechanica 137 (3-4) (1999) 137–149.

[37] W. Zielke, Frequency-Dependent Friction in Transient Pipe Flow, Journal of Basic Engineering 90 (1) (1968) 109–115.

Post-print version of the article: J. Schmidt, W. Kemmetmüller, and A. Kugi, “Modeling and static optimization of a variable speed pumped storage power plant”, *Renewable Energy*, vol. 111, pp. 38–51, 2017. DOI: https://dx.doi.org/10.1016/j.renene.2017.03.055
The content of this post-print version is identical to the published paper but without the publisher’s final layout or copy editing.